Geomorphology 134 (2011) 102–117

Contents lists available at ScienceDirect

Geomorphology

journal homepage: www.elsevier.com/locate/geomorph

The Dead Sea sinkhole hazard: Geophysical assessment of salt dissolution and collapse

Amos Frumkin [a,*], Michael Ezersky [b], Abdallah Al-Zoubi [c], Emad Akkawi [c], Abdel-Rahman Abueladas [c]

[a] Geography Department, The Hebrew University of Jerusalem, Israel
[b] Geophysical Institute of Israel, 6 Baal Shem-Tov Street, Lod 71100, Israel
[c] Al-Balqa Applied University, Salt 19117, Jordan

ARTICLE INFO

Article history:
Received 2 September 2010
Received in revised form 25 March 2011
Accepted 22 April 2011
Available online 30 April 2011

Keywords:
Salt karst
Sinkhole hazard
Dissolution
Collapse
Dead Sea level
Cavity detection

ABSTRACT

A geophysical approach is presented for analyzing processes of subsurface salt dissolution and associated sinkhole hazard along the Dead Sea. The implemented methods include Seismic Refraction (SRFR), Transient Electromagnetic Method (TEM), Electric Resistivity Tomography (ERT), and Ground Penetration Radar (GPR). The combination of these methods allows the delineation of the salt layer boundaries, estimating its porosity distribution, finding cavities within the salt layer, and identifying deformations in the overlying sediments. This approach is shown to be useful for anticipating the occurrence of specific sinkholes, as demonstrated on both shores of the Dead Sea. These sinkholes are observed mainly along the edge of a salt layer deposited during the latest Pleistocene, when Lake Lisan receded to later become the Dead Sea. This salt layer is dissolved by aggressive water flowing from adjacent and underlying aquifers which drain to the Dead Sea. Sinkhole formation is accelerating today due to the rapid fall of the Dead Sea levels during the last 30 years, caused by anthropogenic use of its water.

1. Introduction

Sinkhole hazard is common in limestone karst, associated with collapse or subsidence which often end the life cycle of subsurface cavities (e.g. Klimchouk, 2005; Brinkmann et al., 2008; Frumkin et al., 2009a; Parise et al., 2009). Clusters of sinkholes in limestone karst terrains commonly develop and modify during long periods (in geological time scale). Much faster dynamics, in the order of human life, is commonly attributed to sinkholes formed in evaporitic areas (Gutiérrez et al., 2007), where dissolution rates are one to three orders of magnitude faster compared with limestone.

Evaporites vary largely in their solubility and dissolution rates. Salt (halite, NaCl), a common mineral and rock at the subsurface, is >100 times more soluble than gypsum. Salt is soluble when in contact with the vast majority of environmental water. Therefore, sinkhole hazard related to subsurface dissolution of salt and collapse of overlying material may be extremely large. Salt outcrops are rare and produce typical vadose karst characterized by localized sinkholes, blind valleys and underground streams (e.g. Frumkin, 1994a; Bruthans et al., 2009; De Waele et al., 2009). Geomorphic changes, including sinkhole development, can be extremely rapid particularly in areas where human activities alter groundwater circulation (Lucha et al., 2008). Sinkhole hazards are more commonly associated with dissolution of a covered or mantled salt bed (Ford and Williams, 2007).

Gutiérrez et al. (2008) propose a phased approach for the identification, investigation, prediction, and mitigation of sinkholes in evaporate terrains. Probabilistic sinkhole modeling for hazard assessment and sinkhole susceptibility mapping were attempted for evaporate karst (Galve et al., 2009a,b). Sinkholes are surface manifestation of subsurface dissolution and internal erosion and deformation, commonly hidden from direct observation and from most subaerial geomorphological study methods (Gutiérrez, 2009). Consequently, geophysical methods are indispensable for understanding subsurface mechanisms involved in the development of dissolution-induced sinkholes, and salt karst provides a rapidly evolving sinkholes system to test the geophysical methods.

1.1. The sinkhole hazard along the Dead Sea

During the last 30 years hundreds of sinkholes have occurred along the Dead Sea (DS) shores in both Israel and Jordan (Fig. 1) (e.g. Arkin and Gilat, 2000; Frumkin and Raz, 2001). The process began in the southern part of the Dead Sea coast and spread northward along the western coast. The steeper eastern coast has been less affected, and most of its sinkholes are concentrated in the flat-lying region close to the Lisan Peninsula (Fig. 1).

The sinkholes have already caused considerable damage to infrastructure, and at least four people have fallen into sinkholes which

* Corresponding author.
E-mail addresses: msamos@mscc.huji.ac.il (A. Frumkin), mikhailez@hotmail.com (M. Ezersky), al-azoubi@bau.edu.jo (A. Al-Zoubi).

0169-555X/$ – see front matter © 2011 Elsevier B.V. All rights reserved.
doi:10.1016/j.geomorph.2011.04.023

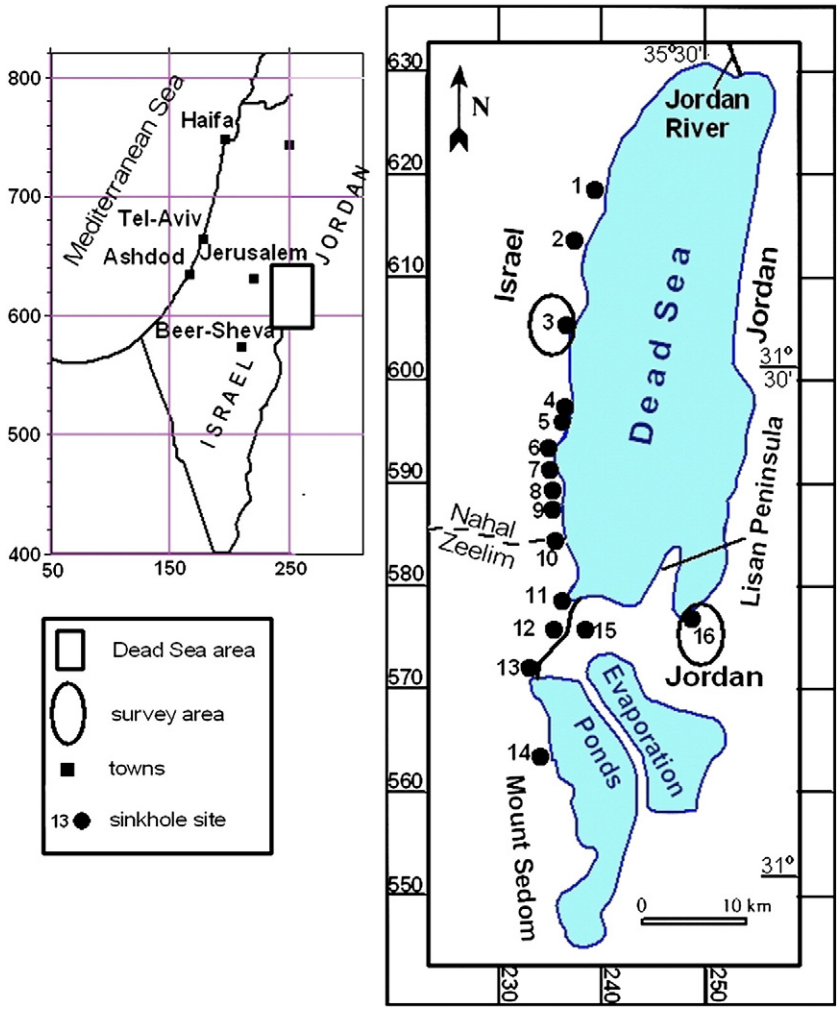

Fig. 1. Sinkhole sites along Dead Sea shore: 1 — Palms, 2 — Samar Spring, 3 — Shalem-2 and Mineral Beach study area, 4 — Ein Gedi and Nahal Arugot, 5 — Yesha, 6 — Zeruya, 7 — Nahal Hever northern, 8 — Nahal Hever southern, 9 — Asa'el, 10 — Nahal Zeelim, 11 — Mezada, 12 — Rahaf, 13 — Mor, 14 — Newe Zohar, 15 — Lisan Peninsula, 16 — Ghor Al-Haditha study area. Coordinates in km, new Israel Transverse Mercator grid.

collapsed under their feet. There is an obvious potential for further collapse beneath the main highways and other human structures. Thus a high sinkhole hazard threatens human lives and future economic development in the Dead Sea basin.

Sinkhole hazard assessment should play a crucial role in planning and development of areas susceptible to sinkhole formation. In order to protect human life and infrastructure, it is necessary to understand how sinkholes form and to produce reliable sinkhole susceptibility and hazard maps identifying the most dangerous areas that should be avoided or properly engineered. However, the DS sinkhole formation mechanism and distribution are only partly understood.

Subsurface cavities and the processes that lead to the development of sinkholes cause changes in the subsurface (porosity, fracture density, water saturation, etc.). These changes may be detected by geophysical methods such as gravity, seismics or electrical resistivity (Ezersky et al., 2006).

Geophysical methods are widely used for karst detection in carbonate karst, e.g. GPR and microgravity (Crawford et al., 1999; Thomas and Roth, 1999) and geoelectric methods (Erchul, 1993; Zhou et al., 1999). A comprehensive review on the geophysical methods used in karst is given in Benson and Yuhr (1993).

Although methodologies for the detection of cavities and other karst features in carbonate rocks (mostly limestone), have received much attention worldwide (Beck and Herring, 2001; Beck, 2003) these techniques need to be adapted, or new methods should be developed, for investigating salt environments such as the evaporite deposits along the Dead Sea coast in Jordan and Israel. Some of the main peculiarities of the unconsolidated, salty sediments in the Dead Sea region are high salinity groundwater and the rapid subsurface dissolution of the salt in response to human-induced changes in environmental (hydrogeological) conditions.

Rapid dissolution explains the high probability of occurrence of sinkholes, and allows assessing (testing) the reliability of geophysically based predictions.

In addition, favorable ground conditions for applying some geophysical methods are met in the DS coastal area. For instance, seismic wave velocity of salt in the DS basin area is considerably higher than that of the host sediments. It permits mapping the salt formation with a high level of confidence (Ezersky, 2006). The very low electrical resistivity of the DS aquifers in the coastal area creates a contrast with surrounding sediments. It permits accurate location of the top of the DS brine with resistivities of 0.5 Ω m to 1 Ω m, and to distinguish it from the fresh water (Goldman et al., 1991; Kafri et al., 1997). Anomalously high resistivity in sinkhole and cavity sites was discovered in alluvial fans in Israel and Jordan (Al-Zoubi et al., 2007; Ezersky, 2008). It allows identifying sinkhole hazardous zones (Frumkin et al., 2009b). Furthermore, it suggests promising conditions for applying the GPR technique to detect subsurface signs of sinkhole development.

A multi-approach geophysical study has been carried out in several sinkhole areas during the last decade (Rybakov et al., 2001;

Eppelbaum et al., 2008; Legchenko et al., 2008a,b; Ezersky et al., 2010). New geophysical methods are under development and new objectives are met (in the framework of Project M27-050 granted by MERC Program). The main objectives of the study are: (1) development of geophysical instruments and methods for investigating various aspects of sinkhole formation; (2) development of an integrated approach for predicting the spatial distribution of future sinkholes in the Dead Sea region based on multiple surface geophysical methods; and (3) testing the sinkhole formation mechanisms proposed in the literature.

This paper examines the potential of geophysical investigation for sinkhole prediction in salt karst and its recent application on both sides of the northern basin of the Dead Sea (Fig. 1). The newly acquired data allow better understanding of sinkhole formation in an area underlain by salt deposits and affected by rapid human-induced hydrological changes.

1.2. The Dead Sea basin: background

The Dead Sea pull-apart morphotectonic basin has formed since the Late Miocene (Garfunkel and Ben-Avraham, 1996; Frumkin, 2001), accumulating clastic and evaporitic sediments up to the present time. The depression is bounded by normal and strike-slip faults.

The structures that control the escarpment consist of steep parallel faults with an overall throw of hundreds of meters. Larger faults are buried under the depression's sedimentary fill, reaching a total vertical throw of several km (Garfunkel and Ben-Avraham, 1996), and down-faulting Cretaceous to Quaternary beds.

The bedrock stratigraphy in the western fault escarpment and adjacent canyons mainly comprises late Cretaceous carbonates. These rocks constitute the aquifer which carries groundwater from the wetter Judean Mountains into the Dead Sea depression that acts as the regional base level (Ben-Itzhak and Gvirtzman, 2005). On the eastern fault escarpment Precambrian to Cretaceous rocks crop out, hosting several aquifers which drain to the Dead Sea.

The DS depression has been occupied by various lakes, the latest being the late Pleistocene Lake Lisan and the Holocene Dead Sea. The Lisan Formation contains alternations of detrital and aragonitic lamina, as well as conglomerates, clays, and evaporites (Begin et al., 1980). Lake Lisan stands were highest just before the last glacial maximum (Bartov et al., 2002; Lisker et al., 2009). Since then until the end of the Pleistocene, Lake Lisan receded abruptly, concurrently with the deposition of a salt layer around 11,000–10,000 years ago (Stein et al., 2010). This latest Pleistocene salt layer ranges from a few meters to a few tens of meters in thickness, lying sub-horizontally some tens of meters under the present surface of the Dead Sea coast.

Close to the Pleistocene–Holocene transition the basin was inundated again, this time by the Dead Sea. During most of the Holocene, the lake level was at ca. −400 m, with small oscillations (Frumkin, 1997; Bookman et al., 2004). This was followed by a recent ongoing drop to ca. −424 m relative to the m.s.l., due to anthropogenic use of water from the lake and its catchment, during the last few decades.

The Holocene sediments of the Dead Sea basin include lacustrine and fluvial facies (Migowski et al., 2006): aragonite-detrital laminar alternations, clastics, and evaporites, mostly of low mechanical strength. The changes in permeability across the stratigraphic sequence often divide the coastal aquifer into several sub-aquifers. In general, the coastal aquifer water is not fresh, but is less salty than the Dead Sea, so it is undersaturated and aggressive in respect to salt. A brackish–saline water interface commonly underlies the coastal aquifer, with much saltier water underneath (Frumkin and Raz, 2001; Yechieli et al., 2006). The recent drop in the Dead Sea level is accompanied by the lowering of the groundwater level and by the expansion of the fresh water zone in the coastal aquifer (Yechieli, 2000). This aquifer is developed within the recent sediments of the basin, receiving the water mainly from the mountain aquifer, and to a lesser degree from ephemeral streams flowing into the Dead Sea. It has been assumed that most water flowing into the coastal aquifer comes from below, under artesian conditions, or by lateral flow from the mountain aquifer at the west. Local annual rainfall is only ~50–100 mm while potential evapotranspiration is >2000 mm, so local rainfall infiltration does not constitute a significant contribution. Temperature is mild in winter and extremely hot in summer (~45 °C several days a year).

2. Sinkhole formation models

Before the 21st century there had been little study and knowledge related to the DS sinkhole-forming processes. During the last decade, several types of approaches were applied to explain sinkhole formation along the Dead Sea, and some of the main ones are briefly discussed below.

2.1. Geomorphic mechanisms

Early studies have suggested two main geomorphic mechanisms to explain the formation of the DS sinkholes:

- piping (Arkin and Gilat, 2000);
- salt dissolution (Frumkin and Raz, 2001).

These mechanisms provided alternative interpretations for the formation of voids at depths of tens of meters within the coastal deposits. During the last decade, boreholes drilled in seven sinkhole clusters along the Dead Sea have penetrated a salt layer, and some of these boreholes encountered cavities within the salt (Yechieli et al., 2002; Abelson et al., 2006). Today it is generally accepted that the DS sinkholes are caused by dissolution of a buried salt layer below the water table, promoted by progressive lowering of the Dead Sea level (Abelson et al., 2006; Shalev et al., 2006; Yechieli et al., 2006; Ezersky et al., 2010).

When the Dead Sea level was high, until the 1970s, the salt layer was in contact with a brine, chemically saturated with respect to salt. According to the salt dissolution mechanism, the drop in Dead Sea level results in lowering of the brackish–saline water interface, allowing the salt to be dissolved by brackish, aggressive water. Thus, the occurrence of sinkholes depends upon the location of the salt layer with respect to the brackish groundwater zone. This mechanism suggests continuous formation of salt cavities in the subsurface during tens of years, as indicated by the timing of sinkhole formation with respect to the recent fall of DS level.

Abelson et al. (2003) suggested that sinkholes tend to develop along faults, which serve as preferential hydraulic pathways, bringing confined aggressive water upwards to contact with salt. A similar mechanism was considered by Closson (2005) for the Jordanian Dead Sea coast. Numerous faults widely distributed through the DS coastal area have been reported by different researchers (e.g. Garfunkel and Ben-Avraham, 1996; Shamir, 2006), whereas sinkholes are usually developed in a single narrow strip 50–100 m wide, roughly parallel to the DS shore.

2.2. Salt dissolution quantitative model

A seismic refraction survey (Ezersky and Legchenko, 2008) showed that the intensive sinkhole development strip coincides with the edge of the salt layer. The working hypothesis is self-acceleration of groundwater circulation, dissolution, and permeability (Bernabé et al., 2003). This process of positive feedback can be described as:

$$\kappa = \kappa_0(\phi/\phi_0)^n \quad (1)$$

Where k_0 and ϕ_0 are the initial permeability and porosity, respectively, k and ϕ are the current permeability and porosity, and n is an empiric constant in the range of 2–3 and over, depending on the sediment. It can be as high as 5 for salt (Bernabé et al., 2003). Thus in accordance with this model, salt dissolution proceeds continuously

as porosity increases in a wide range of values (from few percents up to tens of percents).

Shalev et al. (2006) applied this mechanism to the DS salt dissolution by transverse, cross-formational flow. These authors consider salt dissolution by undersaturated hypogenic groundwater (with halite concentration less than half of that in the Dead Sea water) rising through faults from the deep aquifers. The model requires that the faults or differential compaction should be active to disrupt the underlying clay layers and to keep fault permeability high. A cavity forms where a fault crosses the salt layer. Porosity may rise from zero to 40% (when a cavity is formed) during ~20 to 30 years.

Where the clay aquiclude layers are non-continuous, the salt layer can be directly attached to the gravel aquifer, and dissolution may not be linked to a fault (Shalev et al., 2006). Sinkhole development along the salt edge, with no direct relation to any fault, has been demonstrated by seismic refraction surveys in most of the ten investigated sites of the western DS coast (Ezersky, 2003, 2006; Ezersky et al., 2007, 2010).

2.3. Model based on geophysical studies

The results of recent studies show that: (1) sinkholes are formed within a narrow strip 50–100 m wide along the edge of the salt layer (Ezersky, 2006; Ezersky et al., 2007); (2) collapse breccias (up to tens of thousands of cubic meters) are inferred within the salt layer at sinkhole development sites prior to the occurrence of surface collapse (Eppelbaum et al., 2008; Legchenko et al., 2008a; Ezersky et al., 2010); (3) geomorphic and geophysical monitoring of sinkhole-affected areas carried out in Israel and Jordan revealed that when sinkholes form, cavities are filled with unconsolidated sediments, locally reducing hydraulic conductivity and dissolution (Ezersky et al., 2008, Legchenko and Ezersky, 2009); and (4) groundwater salinity along the Dead Sea shore varies insignificantly. The resistivity of the DS aquifer remains ~0.5 Ω m (Ezersky et al., 2010). Variations of the electrical conductivity in the subsurface revealed by Transient Electromagnetic (TEM) measurements are commonly related to lithological variations caused by collapse structures and sinkholes (Ezersky and Legchenko, 2009; Legchenko et al., 2009). The TEM results were recently confirmed by the geochemical monitoring of borehole water (Yechieli, 2007).

To explain the available field observations Legchenko et al. (2008b) suggested the following model: (1) slow dissolution of salt (longer than 20 years) with possible formation of cavities; (2) sinkhole development triggered by the lowering of the groundwater level, reducing the buoyant support of the overlying sediments; and (3) the timing of sinkhole appearance is also controlled by the mechanical properties of the stoping (upward propagation of cavities by progressive roof breakdown) sediments.

2.4. Geophysical objectives and methodology

The geophysical methodology applied to investigate the sinkholes related to salt dissolution along the DS coasts can be divided into two depth-related objectives:

1. Investigation of relatively deep (25–70 m) processes and factors: salt and aquifer properties, their interaction and salt dissolution;
2. Investigation of shallow (<25 m) subsurface materials and collapse structures generated by stoping, associated with the limited mechanical strength of some DS sediments above deeper dissolution voids.

Consequently, the following geophysical methodology for sinkhole susceptibility assessment in the Dead Sea shore area is considered in this paper:

1. Delineating the salt layer distribution, and particularly the salt edge, based on seismic refraction method;
2. Investigating the depth and thickness of the salt layer using seismic refraction and Transient Electromagnetic (TEM) method;
3. Estimating salt porosity and permeability using bulk resistivity ρ_x measured by TEM method;
4. Investigating the shallow subsurface conditions:
   (a) Assessment of soil decompaction based on Electric Resistivity Tomography (ERT);
   (b) Detection of signs of shallow gravitational deformations (voids, faults, subsidence, synforms, buried sinkholes) based on Ground Penetration Radar (GPR).

3. Study sites

Two representative sites were selected for the present study: Shalem-2 on the western Dead Sea coast, and Ghor Al-Haditha on the eastern coast (Fig. 1). These sites include some of the most common sinkhole features of the Dead Sea region.

3.1. Shalem-2 study site

The Shalem-2 site (also called 'Mineral'), covering ~1 km^2, is located at the western coast of the central part of the northern DS basin (Fig. 1), between the Dead Sea shoreline and Route #90 (the main road along the western DS shore) (Fig. 2). The area comprises the Mineral Spa, where natural black mud and sulfur-rich hydrothermal water with a temperature of 39 °C attract tourists from Israel and abroad. Around Mineral Spa, sinkholes develop in both mudflat (south) and alluvial fan (north) areas.

Figs. 2 and 3 illustrate that sinkhole distribution is mainly linear, possibly along a salt layer edge or controlled by a fault. A salt layer with a cavity was intersected by Mn-2 borehole (Fig. 2). Groundwater sampled from the cavity indicated salt dissolution; Na/Cl ratio of 0.55–0.60 compared with 0.30 in Dead Sea brines (Yechieli et al., 2006). Soon after drilling, the borehole structure collapsed into a newly developed sinkhole which was then east of the salt layer front. Fig. 4 shows that the western edge of the salt is located in alluvium composed of gravel, sand, and clay. These sediments permit direct contact of the salt layer with highly mineralized (200 g/l chloride) rising water at a temperature of 29–40 °C.

Sinkholes are located close to the salt edge. Further to the west, Mn-1 borehole did not cross the salt layer (Fig. 4). This borehole located west of the salt edge revealed aggressive water with relatively low chloride concentration — 120 g/l (Yechieli et al., 2006). Fig. 5 presents a sinkhole between boreholes Mn-1 (W) and Mn-2 (E) as observed on January 2008.

The large cluster of sinkholes south of Mineral Spa started to develop in 1992 (Fig. 3). During recent years sinkhole development progressed northward.

This required delineating a sinkhole susceptibility zoning, which motivated the present geophysical study.

3.2. Ghor Al-Haditha study site

Ghor Al-Haditha is an almost flat area located in the south-east coast of the northern Dead Sea basin (Fig. 1). The altitude is −370 to −390 m below mean sea level. The platform in which sinkholes and subsidence have occurred is a gently inclined wave-eroded platform, about 3 km in width, east of the Lisan Peninsula. The area is typically covered by a thin surface cover of soil and alluvium (Fig. 6a) deposited by Wadi Ibn Hammad (Fig. 7).

Sinkholes at the eastern coast of the Dead Sea have formed since the mid 1980s (Taqieddin et al., 2000). Fig. 7 shows that sinkholes at Ghor Al-Haditha are arranged along a sinuous line with a general NNE–SSW trend.

The geological section shown in Fig. 6b is based on boreholes BH-1 and BH-2 (Taqieddin et al., 2000). Borehole logs indicate that the

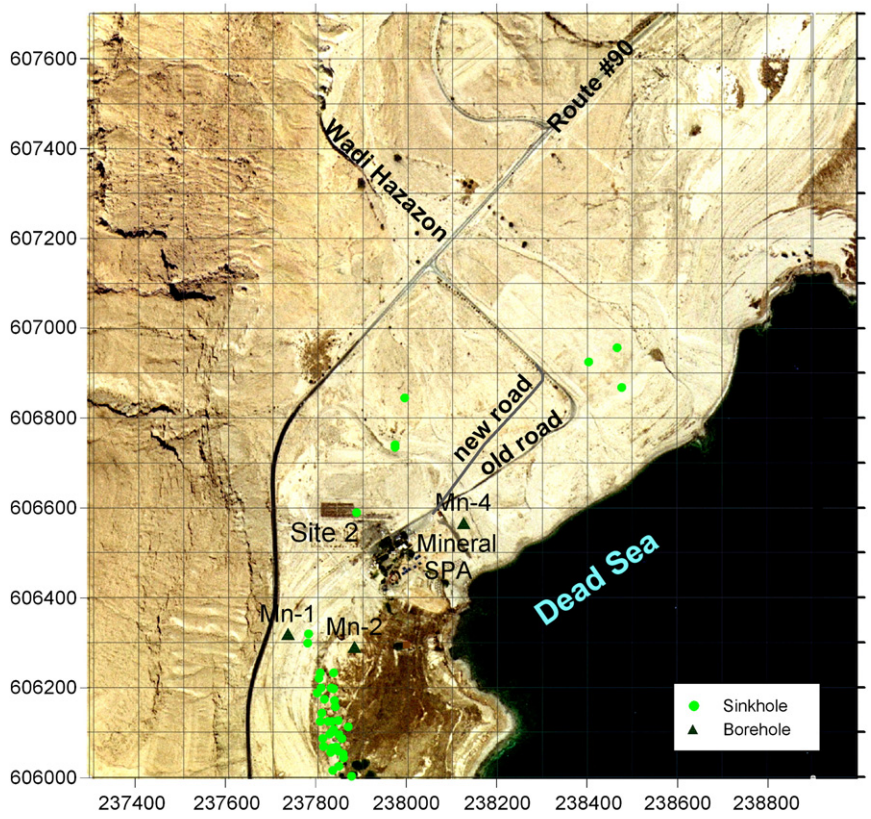

Fig. 2. Mineral Beach (Shalem-2) sinkhole orthophoto. Coordinates are in m, new Israel Transverse Mercator grid.

shallow subsurface sediments consist of laminated calcareous clays interbedded with layers of salt (halite) and gypsum. Salt was encountered in both boreholes, below 32 m at BH-2, and below 47 m at BH-2.

The exposed walls of sinkholes also demonstrate that near surface sediments are mainly composed of sand, silty sand and gravel. The uppermost deposits are similar to those of western DS shore (e.g. Shalem-2).

In the northern sector of Ghor Al-Haditha, sinkholes are scattered on a wider area compared with the south part (Figs. 7 and 8). Slight promotion of sinkholes to the Dead Sea direction was noted in 2007.

4. Methods

We combine several geophysical and field methods that yield information about salt distribution, voids within the salt, and deformation in sediments above the salt. The following surface geophysical methods are jointly applied: Seismic Refraction (SRFR), Transient Electromagnetic (TEM), Electric Resistivity Tomography (ERT) and Ground Penetration Radar (GPR). In our previous studies we used also Magnetic Resonance Sounding (MRS) and Microgravity (see Eppelbaum et al., 2008; Legchenko et al., 2008a, Ezersky et al., 2010 for details). Below we describe the methods used for the present study.

4.1. Seismic Refraction method

Seismic Refraction (SRFR) measurements are used to delineate the edge of the salt unit. Because the salt in the DS area is characterized by a higher P-wave velocity (V_p) than the surrounding sediments, SRFR can be used for salt detection. Comparing boreholes and SRFR data we established a threshold of V_p>2900 m/s for identifying buried salt (Ezersky, 2006); V_p of salt in the DS basin area is 2900–4000 m/s, while its surrounding sediments velocity is 2100–2700 m/s. This threshold remains valid after acquiring a great deal of new data in the Dead Sea region. The refraction data were collected using a 96-channel Summit II Plus seismic recorder of DMT Inc (Germany). From these, 48 channels were used in our studies. The DIGIPULSE source was applied at five shot points on every refraction line (Palmer, 1986).

Seismic refraction waves permit the detection of layers in the subsurface as long as deeper layers have higher V_p than the overlying ones. However, if the deeper layers have a lower velocity than that of the material from which the wave is emerging (i.e. V_2 is less than V_1, a velocity inversion) then the refracted wave will bend towards the perpendicular. This gives rise to a situation known as a hidden layer. That is why seismic refraction waves cannot detect dissolution cavities located at the bottom of the salt layer when they are filled with water or sediments with V_p velocities lower than that of the salt.

4.2. Transient Electromagnetic Method (TEM)

Transient Electromagnetic Method (also referred to as the Time Domain Electromagnetic Method) is used here to estimate the porosity of the salt under the water table. TEM is sensitive to the bulk resistivity (or conductivity) of the studied medium, especially in the low-resistivity range. The TEM method is usually used for vertical depth sounding. A common procedure for ground exploration using transient techniques is laying a square loop in the vicinity of the area to be examined. A *quasi 3D* technique based on numerous 1D soundings was used to map variations in resistivity throughout the area (Barsukov et al., 2006). The TEM FAST 48 HPC system (AEMR, Netherlands) was used with coincident transmitter/receiver square

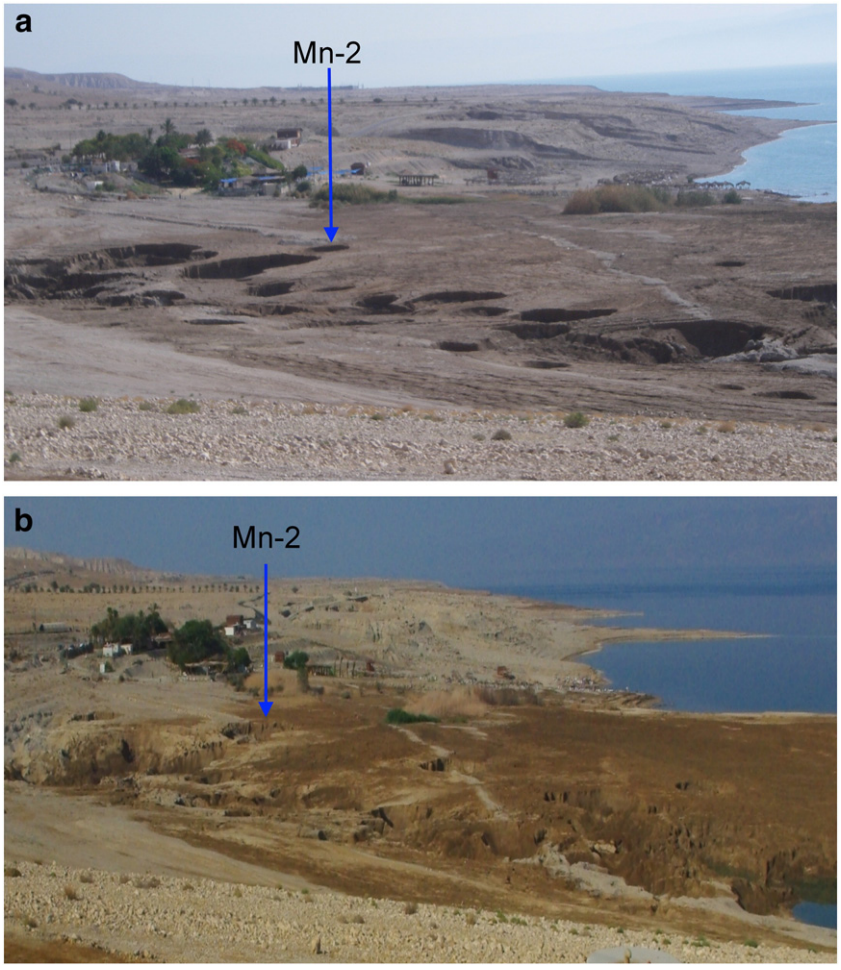

Fig. 3. Sinkhole development over a time interval of 4 years at Shalem 2 site, south of Mineral Spa (background). Sinkholes increase in number and size, and advance northward, along the salt edge. The Mn-2 borehole became a sinkhole east of the main line. (a) View northward on May 2006; (b) Same view on August 2010.

loops with sides of 25, 50 and 100 m. TEM measurements were interpreted using two commercial 1D inversion programs IX1D and TEM Researcher.

Interpretation of the resistivities is based on Archie's Law (Archie, 1942), which establishes that in a saturated medium with ionic pore water conductivity, the bulk electrical resistivity depends on porosity,

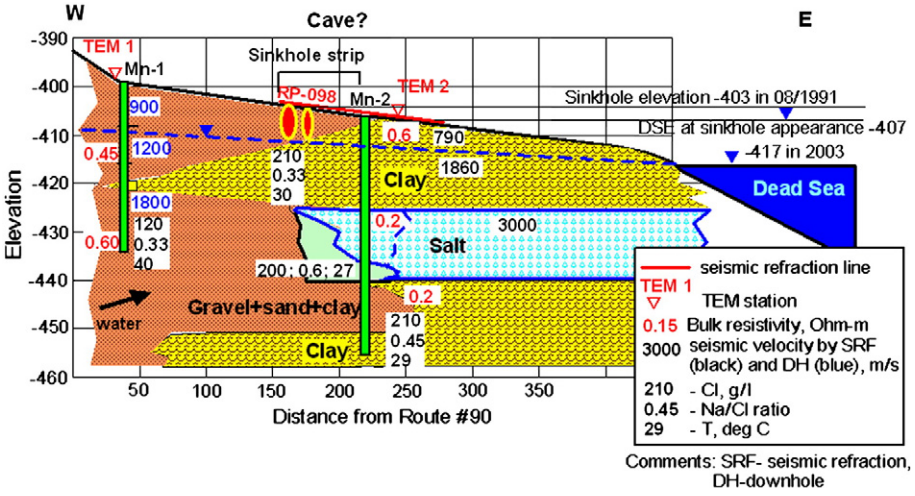

Fig. 4. Composite geological–geophysical section of Shalem-2 (Mineral Beach) based on TEM, seismic refraction, and two boreholes: Mn-1 and Mn-2 (see Fig. 2 for location). Active sinkhole line is represented by ellipses. Water data and TEM bulk resistivity are given numerically. Note that (1) there is direct contact of the salt front with water coming from below and from the west; (2) there is no salt west of sinkholes; salt edge location is defined by the seismic refraction line, and is affected by dissolution (borehole data after Yechieli et al., 2006).

Fig. 5. Sinkhole at the Mineral site between boreholes Mn-1 and Mn-2 on January 2008. Note the collapse of infrastructure, including a road and service pipes.

pore volume occupied by the fluid, and resistivity of the fluid filling the pore space. In this case the bulk resistivity is expressed as:

$$\rho_x = a\,\rho_w\,\phi^{-m} \tag{2}$$

where ρ_w is the resistivity of the solution filling the pores, ϕ is the porosity, parameters a and m appear to depend on the cross-section geometry of the pores along the flow path. The values of parameters a and m vary mostly within the range of 0.6 to 1.4 and 1.37 to 1.95, respectively.

The method has been used extensively in Israel for locating the fresh-saline water interface in coastal areas and for estimating groundwater salinity (Kafri et al., 1997, Kafri and Goldman, 2005). The TEM data are interpreted either qualitatively or quantitatively based on some presumptions. For instance, it is assumed that on constant porosity ϕ of medium values, it is possible to calculate the fluid resistivity ρ_w (functionally connected with the chloride concentration) of groundwater. Such presumption is not always right. It can result in erroneous water salinity assessments (Legchenko et al., 2009). The focus of our study is the porosity of the salt. We presume, based on the model proposed by Shalev et al. (2006), that porosity φ of the salt is laterally decreasing with distance from the salt edge towards the DS. This is because the intensity of water circulation in pores presumably decreases in this direction. Undersaturated water from neighboring aquifers (flowing laterally or through faults from the Judean Mountains and underlying DS sediments) circulating through salt pores becomes saturated with respect to salt in a few days (Frumkin, 1994b). Consequently, fluid resistivity ρ_w will be practically constant and equal to that of the Dead Sea brine, 0.04 Ω m (Kafri and Goldman, 2005). Then bulk resistivity ρ_x in Eq. (2) would therefore be a measure of porosity; higher porosity is associated with lower bulk resistivity. Matching empirical parameters a and m to experimental data, Archie's law for DS salt can be used to estimate porosity from measured resistivity. Spanbenberg et al. (1998)

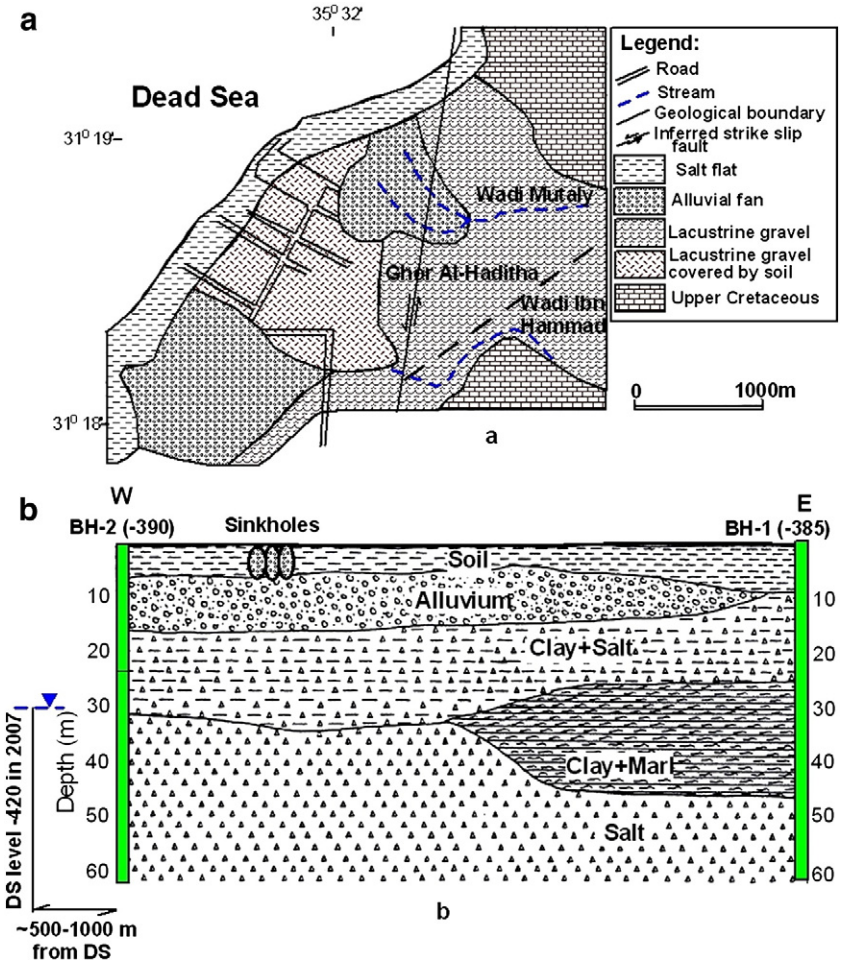

Fig. 6. Ghor Al-Haditha geological setting after Taqieddin et al. (2000). (a) Geological map of the study area; (b) geological section through boreholes 1 and 2 (see Fig. 7 for location).

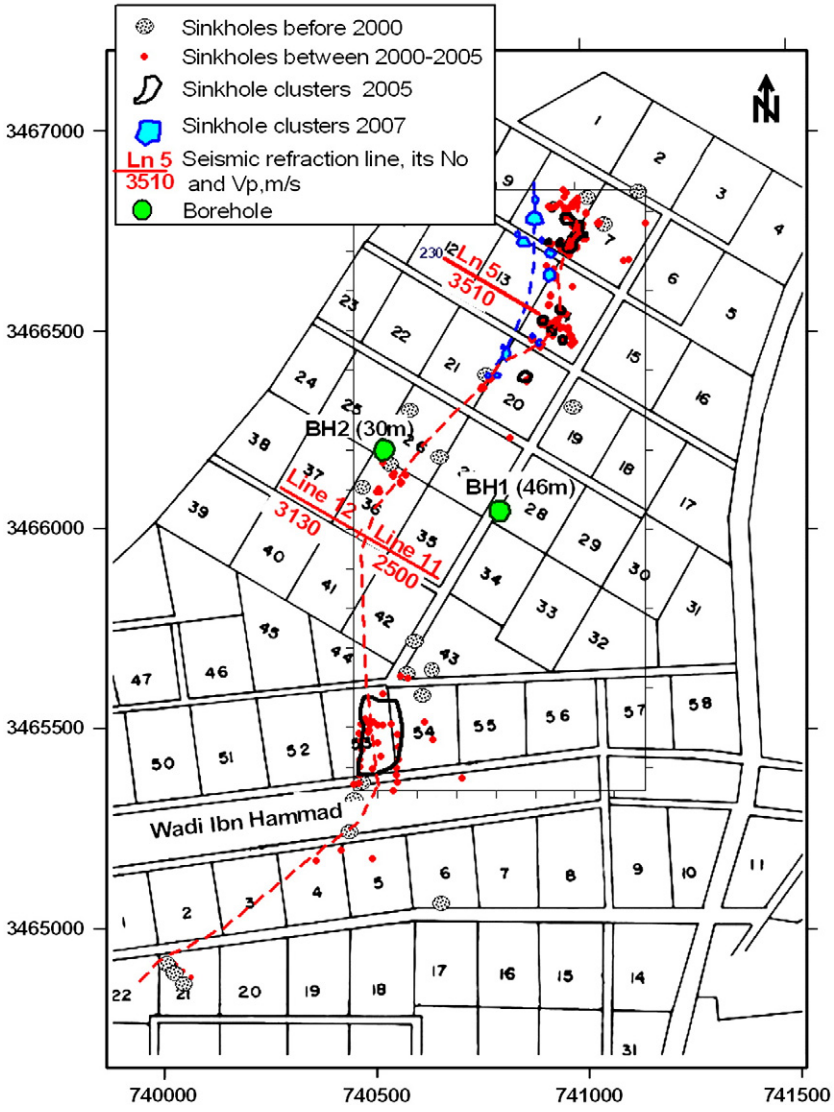

Fig. 7. Ghor Al-Haditha map with seismic refraction lines (after El-Isa et al., 1995), boreholes and sinkholes before 2000 (after Taqieddin et al., 2000), sinkholes between 2000 and 2005, sinkhole clusters in 2005 and 2007 (after Abueladas, pers. comm.). Coordinates in m, Universal Transverse Mercator grid.

Fig. 8. Northern sinkhole cluster of Ghor Al-Haditha in 2010, courtesy of Google Earth. Cultivated fields which were partly abandoned following sinkhole development. DS retreating shore is at the north-west.

proposed the following form of Archie's Law for salt artificial specimens:

$$F = \rho_x / \rho_w = 0.62\,\phi^{-2.33} \tag{3}$$

where $F = \rho_x/\rho_w$ is named the formation factor. This expression provides a rough estimate of salt porosity from bulk resistivity. Nevertheless, it will be shortly checked for the DS salt.

4.3. Electrical Resistivity Tomography (ERT) method

ERT is used here to detect shallow deformations in subsurface sediments. 2D resistivity prospecting yields information about both lateral and vertical distribution of resistivity through the geological section and can therefore be used in both qualitative and quantitative ways for the interpretation of deformation structures at shallow depths. ERT has been used before for this purpose by Loke and Barker (1996). The subsurface resistivity distribution is determined by measurements performed on the ground surface. From these measurements, the distribution of a true resistivity of the subsurface is estimated. The geoelectric method is adopted in geological engineering and hydro-geological applications, because of its high efficiency for detecting the

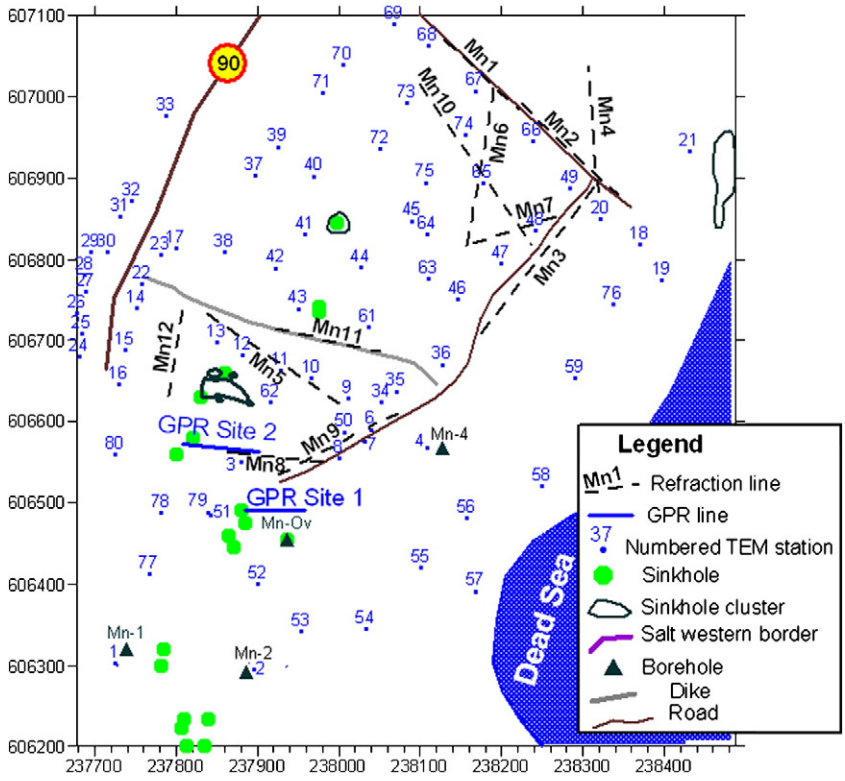

Fig. 9. Seismic line and TEM station layouts at Shalem-2 site. Coordinates in m, new Israel Transverse Mercator grid.

presence of heterogeneities (cavities, ore bodies, etc.). This method can also be used for differentiating layers of clay, marl, sand, sandstone, limestone and water saturated soils and rocks.

The data have been inverted using the RES2DINV software (Loke, 1999). Simple "quasi" 3-D mapping derived from the multiple 2-D lines was carried out through the area using the conventional Wenner electrode array (with equal spacing between electrodes). The measurements were carried out with an IRIS SYSCAL R2 system.

Quantitative interpretation of the results should be based on the *modified Archie's Law*, which establishes that in partially saturated soil with ionic pore water conductivity (above the water table), bulk electrical resistivity depends on the porosity, pore volume occupied by the fluid and the resistivity of the fluid filling the pore space (Zhdanov and Keller, 1994). In case of a partially saturated medium, bulk resistivity will be expressed as:

$$\rho_x = a\rho_w S^{-n}\phi^{-m} \tag{4}$$

where ρ_x, ρ_w ϕ, a and m are the same as those in Eq. (2), $S = V_{el}/V_\Sigma$ is the fraction of the pore space filled with the same electrolyte (named also degree of soil pore filling); V_{el} is the volume of the electrolyte in pores; V_Σ is the total pore volume per unit volume of soil; n is an empirical parameter termed the saturation exponent, which usually has a value of approximately 2.

As follows from the modified Archie's Law, resistivity of the unsaturated sediments is mainly determined by their porosity. The higher the porosity, the higher the resistivity. The bulk resistivity will also depend on the volume of the electrolyte V_{el} in pores and resistivity of the fluid ρ_w. This has been shown using 2D resistivity modeling (Ezersky, 2008). Note that the higher porosity in sinkhole sites is caused by the presence of cavities and collapsed sediments at depth (Maimon et al., 2005). Therefore ERT was first used in the Dead Sea sinkhole areas to detect subsurface high resistivity anomalies caused by the higher porosity of the subsurface sediments (Ezersky, 2003, 2008; Al-Zoubi et al., 2007).

4.4. Ground Penetrating Radar (GPR) method

GPR is used here to detect shallow structural deformations in sediments above the salt layer. GPR is based on the transmission of electromagnetic waves into the subsurface and the recording of reflected waves from objects or interfaces with different dielectric constants. A radar system comprises a signal generator, antennae (for transmission and reception), and receiver. The system has an onboard computer that facilitates data processing both while acquiring data in the field and post-recording (Reynolds, 1997). As the antenna is moved along ground surface, the signals of the reflected waves are displayed as a function of their two-way travel time, i.e. the time elapsed between the transmission and detection by the receiver, in the form of radargram. In low-loss medium the reflection depth of an electromagnetic wave (S) is:

$$S = \frac{t^*C}{2\sqrt{\varepsilon_r}}, \tag{5}$$

where t is the two-way travel time, determined from the radargram, C is the speed of light in free space and ε_r is the relative dielectric constant, which is 1 for air and 81 for water.

For geological applications, where often depth penetration tends to be more important than high resolution, antennas for frequencies of not more than 500 MHz are used. In the present survey we used a SIR-20 GPR system manufactured by GSSI (USA), using 400 MHz, 200 MHz and 100 MHz frequency antennas. WINRAD A/VA 5 software was applied for post processing of the radargrams. Acquisition range was 50 ns (for 500 MHz antenna) and 200 ns (for 100 MHz antenna). The dielectric constant of the DS deposits varies in a wide range from $\varepsilon_r = 3$–6 (alluvial fans) to $\varepsilon_r = 25$–45 (mud flats). Such a wide range is caused by variable soil salinity, from very high at the mud flat sites (where sediments are saturated with DS brine) to very low at the alluvial fan sites (where sediments have a high porosity). However, sinkhole risk is highest at the latter sites where dwellings and roads are located in both Israel and Jordan. Therefore, GPR surveys were carried

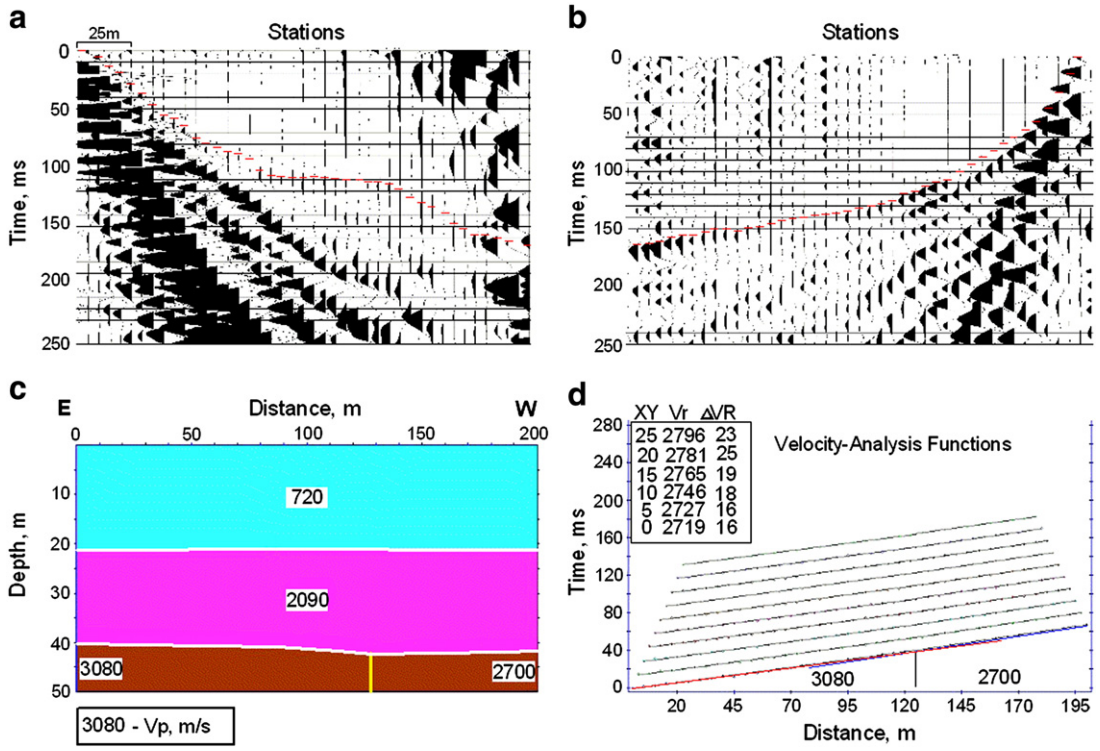

Fig. 10. Results obtained along seismic line MN-5. (a and b) Examples of the reciprocal zero-offsets (high cut filters 125 Hz were applied to the raw data); (c) Depth velocity section; (d) Velocity analysis functions.

out in both countries on alluvial fans (e.g. Batayneh et al., 2002, Ezersky et al., 2006, Frumkin et al., 2009b). In several cases, sinkhole formation by surface collapse followed GPR detection of subsurface voids and deformation (e.g. Arkin et al., 2000; Ezersky et al., 2006).

5. Results

5.1. Delineation of the salt layer edge by seismic refraction

Delineation of the salt layer edge by seismic refraction should be the first step in a sinkhole susceptibility assessment. In Israel, seismic refraction has been carried out using General Reciprocal Method (GRM) (Ezersky, 2006; Ezersky et al., 2010). In Jordan, Common Reciprocal Method (CRM) (Taqieddin et al., 2000; El-Isa et al., 1995), tomography technique (Dhemaied, 2007) and Multichannel Analysis of Surface Waves (MASW) (Bodet et al., 2010) have been applied.

We have mapped the salt border in a sector of the Shalem-2 area employing seismic refraction lines along roads and construction-free areas. The seismic line location as well as TEM stations are shown in Fig. 9. The rough topography of channels, trenches, boulders, and fluvial sediments complicate the area rendering it inaccessible for vehicles.

Nine seismic refraction profiles were shot in a $600 \times 600\ m^2$ area. Examples of the seismic depth–velocity sections obtained at seismic line Mn5 are shown in Fig. 10. The raw data (Fig. 10a and b) are of good quality. Noise was suppressed using a high cut filter of 125 Hz. In the velocity analysis function two blocks are clearly seen (Fig. 10d). Less matching line corresponds to XY = 0–5 m. The depth–velocity section along line Mn5 is represented in Fig. 10c. Two lateral velocity blocks are distinguished

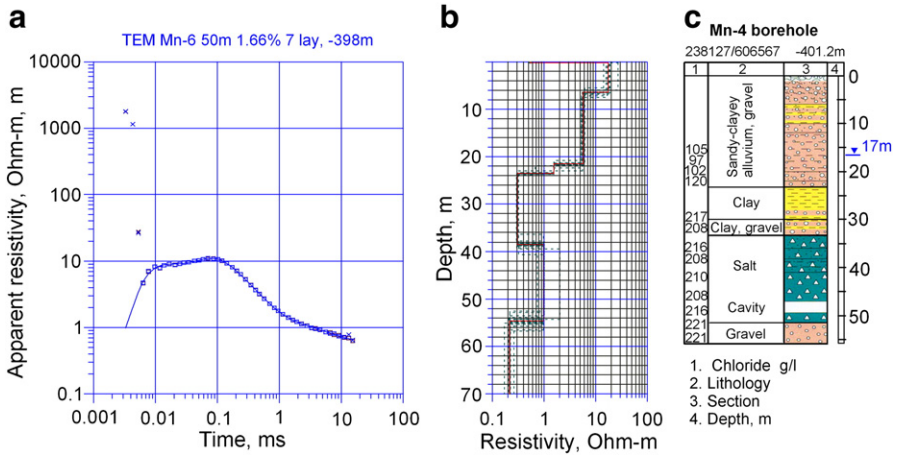

Fig. 11. TEM 6 station ($50 \times 50\ m^2$ loop) results compared with stratigraphy: (a) Apparent resistivity versus time (field record); (b) Inverse resistivity versus depth function; (c) Mn-4 borehole section (see Fig. 9 for location).

below a depth of 40 m: an eastern block ($V_p = 3080$ m/s), 40 m deep, interpreted as a salt layer, and a western block ($V_p = 2700$ m/s) interpreted as clastic sediments saturated with DS brine.

5.3. Salt properties mapping using TEM

It follows from Section 4.3 that knowledge of the Archie's Law for salt allows estimating its porosity. Therefore, salt mapping using TEM is one of the most important parts of the methodology. The idea is to detect a high resistivity layer compared with the very low resistivity background, taking into account that the salt layer is within the saturated zone of the DS brine. Our preliminary laboratory resistivity measurements have shown that the resistivity of the bulk salt specimens saturated with brine is ~4–6 Ω m. It corresponds to ~8–10% porosity of the salt. If fluid resistivity ρ_w within pores does not change, then variations of the bulk salt resistivity ρ_x are determined by variations in the salt porosity ϕ. The bulk resistivity of the brine-saturated salt layer in the DS subsurface varies in the range of 0.5–1.0 Ω m. Detecting this layer, mapping its top and bottom, and determining its resistivity are our objectives. If an aggressive (unsaturated with respect to chloride) fluid enters the salt, it would dissolve salt rapidly, becoming saturated with respect to salt in a short time (Frumkin, 1994b). Therefore the resistivity of the fluid in salt pores is almost constant and very low (~0.04 Ω m). An example of resistivity versus depth measured at the TEM station Mn-6 is shown in Fig. 11b in comparison with the Mn-4 borehole hydrogeology (Fig. 11c).

Fig. 11a shows that the field record (signal) is of good quality from 0.007 to 10 ms (milliseconds). The graph of inverse resistivity versus depth (Fig. 11b) reveals seven layers. Green dotted lines show equivalent solutions, so the red graph can be considered as the most probable model of the resistivity depth function.

The drop in resistivity from 5 Ω m to 1.5–2.0 Ω m at 22 m corresponds evidently to the water table. Water table indicated in the borehole log (Fig. 11c) was measured in 2004 when the borehole was drilled. During the following 5 years water table declined in accordance with the DS level at a mean rate of 1 m/year. The layer of 1 Ω m bulk resistivity at the background of 0.2–0.3 Ω m at a 38–54 m depth range represents the salt layer. The resistivity graph (Fig. 11b) thus allows identifying the depth of the salt top (38 m) and bottom (55 m), measuring the salt thickness (16–17 m) and its average resistivity — 1 Ω m.

Fifty TEM soundings were carried out through the Shalem-2 area (Fig. 9). The resulting salt resistivity map is shown in Fig. 12. The map presents the distribution of the average resistivity of the salt layer throughout the Shalem-2 area. In addition to resistivity, the color scale of Fig. 12 also shows values of porosity revealed from expression (3). These porosity values can give an approximate estimation of salt conditions (e.g. compaction and degree of karstification) based on bulk resistivity. Some characteristic regularities of resistivity distribution can be distinguished in Fig. 12. For instance, resistivity of the salt layer increases (porosity decreases) in the DS direction, while resistivity decreases (porosity increases) towards the salt border. Further studies on resistivity–porosity–permeability relationships based on investigation of salt specimens and boreholes, will give us the possibility to interpret resistivity data quantitatively. The method allows producing isopach maps of salt thickness, and structural maps showing the elevation of the salt top and bottom.

The salt map (Fig. 12) is based on all data acquired through the Shalem-2 site. This map combines seismic refraction with TEM mapping results. These results are corroborated by boreholes which penetrated the salt east of the salt edge depicted in Fig. 12 (Abelson et al., 2006). Note, however, that borehole Mn-2 intersected the salt

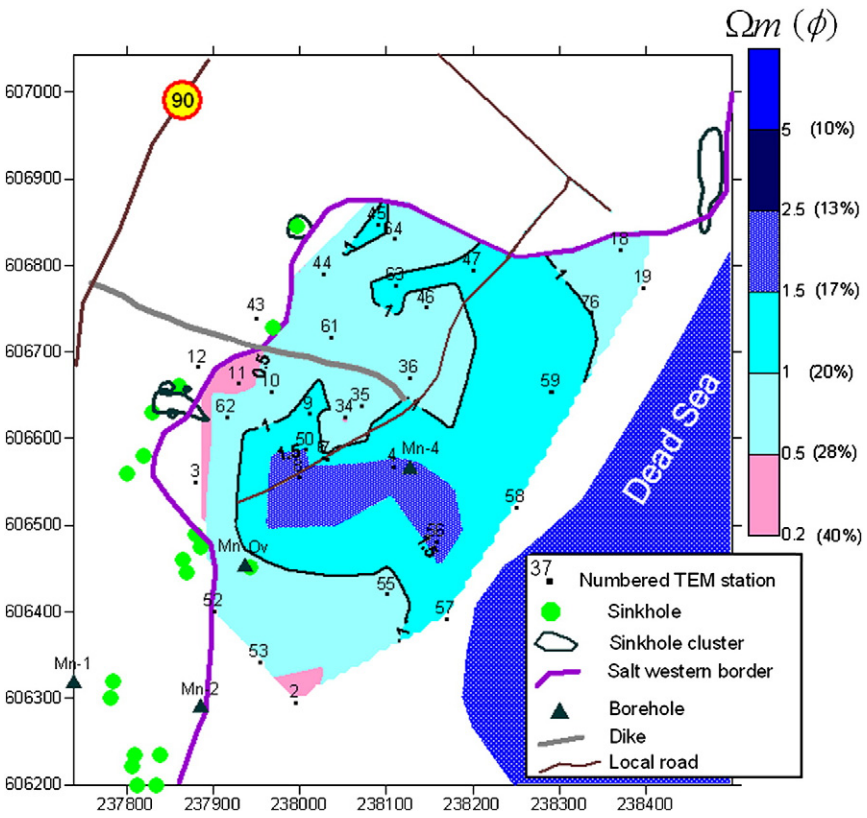

Fig. 12. Salt boundary, average resistivity and estimated porosity (n%) distribution of the salt layer through the Shalem-2 area, based upon combined seismic refraction and TEM results.

layer at −424 m on 2003. Later the borehole structure collapsed into a new sinkhole, and today (2009) the salt border has migrated eastward towards the basin due to rapid dissolution. In general, Fig. 12 shows that sinkholes developed along the salt edge, rather than along other tectonic or sedimentary features.

5.4. Studying shallow subsurface structures using GPR

As shown above, the salt edge is the most hazardous zone where premonitory signs of imminent surface collapse could be detected. Such surface signs can be shallow voids, fractures, faults, subsidence, buried sinkholes, synforms, etc. (Frumkin et al., 2009b).

Here we report our GPR study carried out in the Shalem-2 site 2 to detect hazardous locations along a dirt road connecting the Mineral Spa to Route #90 (Fig. 9). The dirt road runs perpendicular to the salt edge, crossing it at the south-western part of site 2. Geoelectric sounding was first performed to determine the resistivity structure of the site. A resistivity of 120 Ω m characterizes the vadose zone down to 17 m below surface. A 1 Ω m interface separates highly resistive dry alluvial sediments from the DS aquifer. This interface is interpreted as sediments which are partly wetted by capillary rising of salty water from the water table, a process observed directly in sinkhole walls above the water table. The water table is at 18.5 m, below which the resistivity of the DS aquifer is 0.25–0.3 Ω m, characterizing a hypersaline brine filling pores in a clay layer. Thus, the subsurface vadose zone is characterized by relatively high resistivity allowing a GPR penetration depth of 8–10 m at a dielectric constant of 5–6.

Five GPR lines were carried out at site 2 along the dirt road and two additional oblique lines (Figs. 13 and 14a). Antennae of 300 MHz, 400 MHz and 500 MHz were used. On November 2008 the dirt road surface topography along line 1 was smooth (Fig. 14b), with a slight slope 0.2 m high at the western part. Three anomalies can be distinguished in the radargram acquired along line 1 on November 2008 (Fig. 14c).

The western-most anomaly no. 1 (Fig. 14c) corresponds to a vertical structure, apparently a fault or fracture. Anomaly 2 in Fig. 14c reveals a disturbed medium interpreted as fractures and voids filled with air.

Finally, anomaly 3 in Fig. 14c is a strong reflector whose pores can be filled with air or water. Anomalies 2 and 3 reveal an inclined and sagged layer. No signs of sinkholes were seen on the surface on November 2008. The anomalous reflector is shown in the 3D presentation (Fig. 15) generated with the profiles acquired along 5 lines (see location of 5 lines in Fig. 14a).

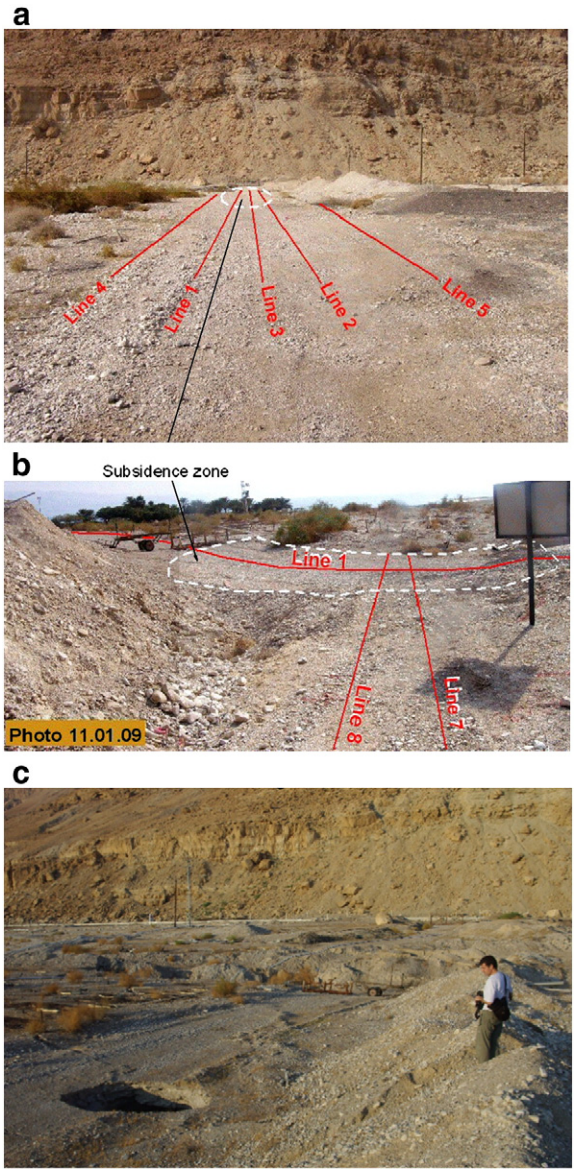

Fig. 13. Shalem-2, GPR Site 2 (for location see Fig. 2). (a) Dirt road connecting Mineral Spa to Route #90 on November 2008 (view to the west): the road was still intact with a regular surface. GPR lines are shown; (b) January 2009: the road is already intersected by an elongated subsidence zone formed close to the salt edge above GPR anomalies 1 and 2 (view to the south); (c) The dirt road (view to the west) on January 2011, following major sinkhole development (compare with a). An elongated subsidence trough (center) has developed above GPR anomalies 1 and 2 of Fig. 14c, above the salt edge. A circular collapse sinkhole (lower left) has recently developed above anomaly 3.

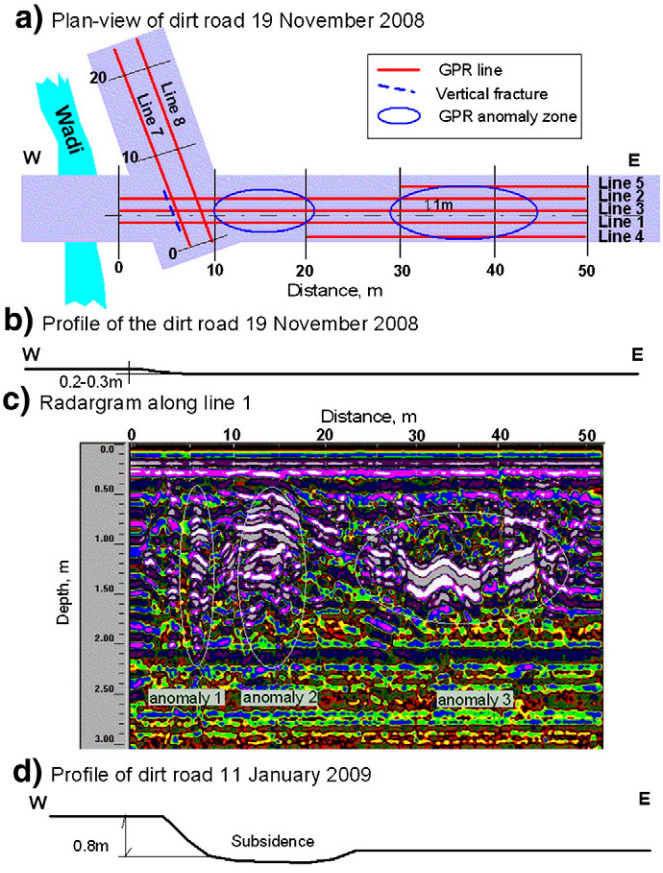

Fig. 14. GPR study at the Shalem-2, site 2. (a) GPR line layout; (b) Topography of the dirt road at the time of study in November 2008; (c) Radargram along central line 1 obtained with a 500 MHz antenna; (d) Topography of the dirt road along line 1 on January 2009. The subsidence belt crosses the dirt road (compare with Fig. 13b).

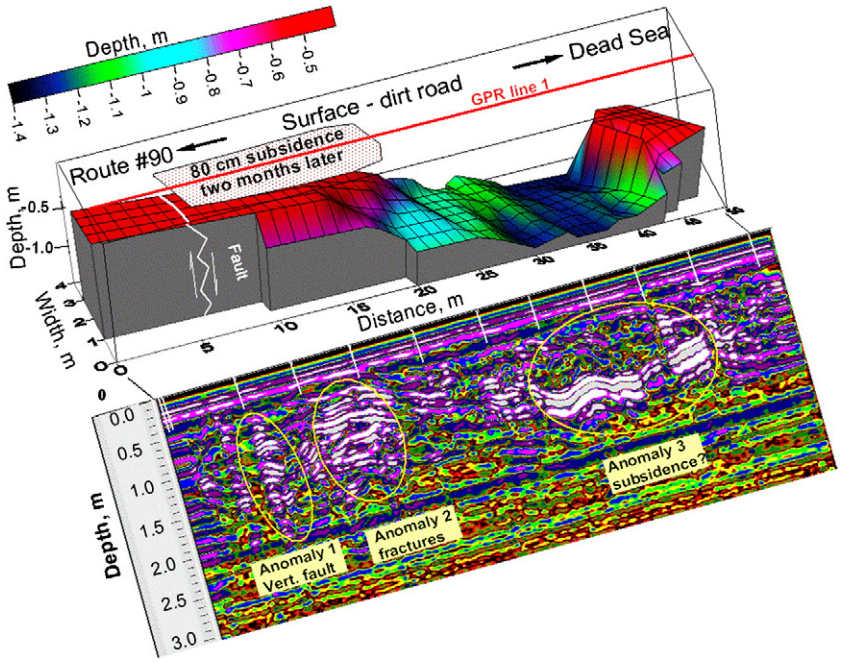

Fig. 15. Three-D presentation of the anomalous reflector detected by the GPR scanning along the dirt road of Figs. 13 and 14.

Two weeks later a sharp scarp formed at the place of anomaly 1 (L. Kofman, Technion R&D, personal communication). By 17 December 2008 the scarp reached 0.8–1.0 m in height, and a new collapse sinkhole was formed.

A sinkhole 5 m in diameter and 2 m deep formed above anomaly 2, and concentric fractures 5–10 mm wide (Fig. 13c lower left) were seen at the surface above anomaly 3 (Fig. 14c). The surface has further subsided at the location of anomalies 1 and 2. Finally, on 21 December 2010, a new 3 m deep sinkhole was observed above anomaly 3 (Fig. 13c). The sinkholes above anomalies 1 and 2 have converged, forming a large subsidence trough above the salt edge (Figs. 13c and 14c). Thus sinkholes have appeared above all anomalies detected earlier by GPR at site 2.

This study illustrates rapid sinkhole development close to the edge of the salt layer at Shalem-2 area. Subsurface anomalies were successfully detected by GPR, providing precursory signs of collapse.

5.5. Studying subsurface structures using ERT

Jordanian researchers have used GPR, ERT, Magnetometry and Microgravity to detect subsurface anomalies, cavities and formations in order to anticipate imminent collapse at Ghor Al-Haditha, following sinkhole development in this area (Fig. 16). Here we present an example of two ERT sections along lines No. 1 and 2 (Fig. 17).

Fig. 16. Recent sinkholes in the Ghor Al-Haditha site, Jordan. Note the ruptured surface at the foreground, indicating that further subsidence is imminent.

A characteristic feature of the section along line ERT 1 is a high resistivity anomaly of 2000 Ω m at 240 m distance and 10–15 m depth. The anomaly contrasts with the low resistivity background of 15–100 Ω m (Fig. 17b). Conversely, ERT 2 section located some 400 m northward shows low resistivity values (1–50 Ω m) throughout the whole section (Fig. 17c). Similar background resistivity is typical for the DS area vadose zone. However, as mentioned above, sites of sinkhole development are characterized by higher resistivity values. Following the results in Shalem-2, we hypothesize that the anomaly detected by line ERT 1 is related to a gradually stoping cavity possibly indicating an imminent sinkhole.

6. Discussion

The main aim of this study is to find an optimal way of integrating several geophysical methods in order to provide a basic sinkhole susceptibility assessment. An additional benefit is a better understanding of sinkhole formation above salt deposits. Indeed, the integration of several methods at Shalem-2 allowed the prediction of sinkhole formation before it actually occurred.

In spite of the various DS sinkhole formation models, most researchers agree that sinkhole development is connected with the drop of the Dead Sea level, either because of aggressive water incursion into the coastal area (Yechieli et al., 2002, 2006), or because of artesian flow via faults and conduits (Abelson et al., 2006, Shalev et al., 2006), or because of collapse of surface sediments into pre-existing dissolution cavities due to decreasing buoyant support (Legchenko et al., 2008b). A combination of these non-exclusive models, which often enhance one another is a probable situation.

The application of geophysical methods to the DS sinkhole problem is based upon the model formulated in our earlier works (Bruner et al., 2003; Ezersky, 2003; Ezersky et al., 2010). The present study, following previous ones, shows that the dissolution process occurs preferentially where the salt and clay lake sediments interfinger with alluvial and colluvial gravel and sand. Further towards the lake, the salt layer is sandwiched within thick fine-grained lake deposits, commonly clay,

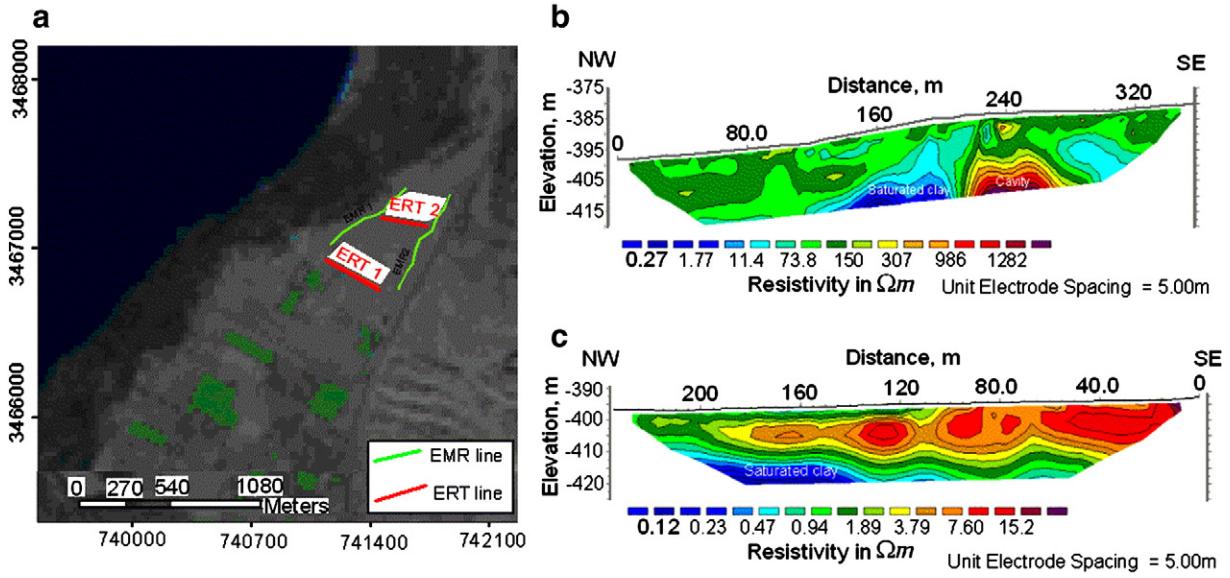

Fig. 17. (a) Location map of geophysical studies; (b) ERT profile 1 at the north of the Ghor Al-Haditha site (distribution of the sinkholes is shown in Figure 7). Note anomaly at 240 m, possibly indicating a gradually stoping cavity where a future sinkhole is expected; (c) ERT profile 2, ~400 m north of profile 1.

acting as hydraulic protective layers above and below the salt. The dissolution zone is thus commonly limited to a fringe along the salt edge and between it and the low permeability zone where Dead Sea clay layers block the underground flow.

The rapid development of a sinkhole at the Mn-2 drilling site (and at other boreholes as well) suggests that dissolution (at least in this site) is dominated by upward flow from a confined aquifer. Wherever the aquiclude layers are perforated, artesian water can rise into the salt, creating dissolution voids rapidly. This is corroborated by higher water pressure at the aquifer underlying the salt, compared with the overlying aquifer (Yechieli et al., 2006), and by sinkholes developed under lake water. For some cases, faults may perforate the aquiclude layers, as suggested by lines of sinkholes perpendicular to the salt edge (Frumkin and Raz, 2001, their Fig. 10). Anyway, the lakeward thickening of clay deposits limit the ability of faults and fractures to perforate these aquiclude layers. The formation of large karstic voids due to rising hypogenic water has become widely appreciated in both carbonates and evaporites (e.g. Frumkin and Gvirtzman, 2006; Klimchouk 2009). In the case presented here, the head of the overlying aquifer has diminished dramatically during the last decades due to the fall of Dead Sea levels, promoting increased artesian flow and rapid dissolution. Salt dissolution may take place a short or long period before any signs are evident on the surface (Fig. 18a). The sinkholes commonly developed along the salt edge which was dissolved by brackish water, unsaturated with respect to chloride (Yechieli et al., 2006, Yechieli, 2007; Legchenko et al., 2009; Ezersky et al., 2010).

Instability of the salt cavity ceiling causes upward stoping through the mechanically-weak sediments situated between the cavity and the surface (Fig. 18b). Ford and Williams (2007, p. 385) report cases in different geological settings, where the stoping process propagated through >1000 m of cover rocks. This intermediate stage continues until the surface collapses and a sinkhole forms (Fig. 18c).

Extrapolating the ongoing retreat of the Dead Sea, the water-table will fall progressively below the salt layer, leaving it within the vadose zone. This situation will favor karstification by downward vadose flow from ephemeral streams (e.g. Frumkin, 1994a).

Considering the above-mentioned processes, we have resolved three important aspects by means of geophysics:

1. Distribution of the salt layer, and particularly its edge;
2. Zones of increased porosity and their lateral distribution throughout the salt area;
3. Changes in the properties and structure of shallow sediments, overlying cavities. These disturbances include increased porosity and various types of ductile and brittle deformation structures (e.g. Yang and Drumm, 2002; Maimon et al., 2005). Porous and

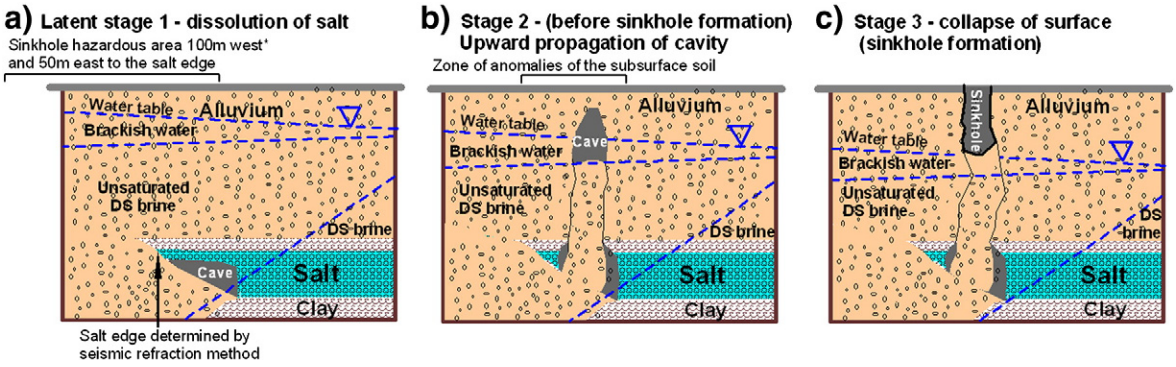

Fig. 18. Three stages of sinkhole formation at the salt edge: a generalized model. Note that although there is not salt west of the present salt edge, salt has been dissolved there earlier. Therefore cavities may still propagate towards the surface. It is confirmed by statistics of sinkhole formation. (a) Latent stage, (b) upward propagation of cavity (stoping); (c) sinkhole formation.

fractured zones in the subsurface detected by geophysical methods (ERT, GPR etc.) may allow anticipating imminent sinkholes before the collapse reaches the surface, allowing for timely warning.

7. Conclusions

The recent development of geophysics has allowed us to combine various methods for delineating salt distribution and voids within the salt, as well as identifying shallow evidence of deformation allowing the anticipation of imminent sinkholes.

Additional data, such as hydrogeology and surface geomorphology are implemented into this methodology and combined to gain a better insight into the processes and factors that control sinkhole development. The rapidity of sinkhole development following the decline of the Dead Sea level allows testing the geophysical assessment presented here by monitoring collapse sinkholes developed at the sites where shallow anomalies along the salt edge were previously detected.

In addition to the geophysical conclusion, our data from the Dead Sea sinkholes provide valuable information on controlling factors and genetic processes of sinkhole formation mechanisms. Dead Sea sinkholes form mainly above areas of subjacent salt dissolution, dominated by confined artesian flow of hypogenic origin. This water is aggressive with respect to salt and often hydrothermal. The location of most sinkholes is determined by the combination of high-permeability layers such as coarse fluvial sediments, and the westernmost edge of the salt layer. So far, sinkholes rarely develop further lakeward, because of the increasingly thicker clay aquicludes bounding the salt layer. The rapid dynamics of the system renders the Dead Sea coastal environment a highly hazardous area for sinkhole formation. The possible remedy of raising the Dead Sea to its mid 20th century level (Frumkin and Raz, 2001) is still being evaluated today.

Based on the above-mentioned evidence one can conclude that salt distribution, DS level, and aggressive water are the main factors determining the salt sinkhole hazard. Geophysical methods are applicable to predict imminent sinkholes and mitigate the hazard.

Acknowledgements

This work was made possible through support provided by the U.S. Agency for International Development, under terms of Award No M27-050. The opinions expressed herein are those of the authors and do not necessary reflect the views of the USAID. We are also grateful to the Ministry of Infrastructure of Israel for supporting this investigation. We are grateful to the Geophysical Institute of Israel and Al-Balqa Applied University staff for the efficient organization and performance of the field work, and to the Tamar Regional Council for supporting this study. Thanks to Lev Kofman for cooperation in the GPR study, and to Eli Raz for useful information about recent sinkhole development. Francisco Gutiérrez has improved the manuscript substantially with a careful review.

References

Abelson, M., Baer, G., Shtivelman, V., Wachs, D., Raz, E., Crouvi, O., Kurzon, I., Yechieli, Y., 2003. Collapse-sinkholes and radar interferometry reveal neotectonics concealed within the Dead Sea basin. Geophysical Research Letters 30, 1545.

Abelson, M., Yechieli, Y., Crouvi, O., Baer, G., Wachs, D., Bein, A., Shtivelman, V., 2006. In: Enzel, Y., Agnon, A., Stein, M. (Eds.), Evolution of the Dead Sea sinkholes: Geological Society of America Special Paper, 401, pp. 241–253.

Al-Zoubi, A., Abueladas, A.-R., Camerlynck, C., Al-Ruzouq, R., Al-Rawashdeh, S., Ezersky, M., Ali, W., 2007. Use of 2D multi electrodes resistivity imagining for sinkholes hazard assessment along the eastern part of the Dead Sea, Jordan. American Journal of Environmental Sciences 3, 229–233.

Archie, G.E., 1942. Electrical resistivity as an aid in core analysis interpretation. Transactions of the American Institute of Mining Engineers 146, 54–62.

Arkin, Y., Gilat, A., 2000. Dead Sea sinkholes — an ever-developing hazard. Environmental Geology 39, 711–722.

Arkin, Y., Gilat, A., Kofman, L., 2000. Developing Dead Sea sinkholes revealed by ground penetrating radar. Geological Survey of Israel Current Research 12, 25–30.

Barsukov, P., Fainberg, E., Khabensky, E., 2006. Shallow investigations by TEM-FAST technique: methodology and examples. In: Spichak, V. (Ed.), Electromagnetic sounding of the Earth's interior. Methods in Geochemistry and Geophysics, 40. Elsevier, Amsterdam, pp. 55–77.

Bartov, Y., Stein, M., Enzel, Y., Agnon, A., Reches, Z., 2002. Lake levels and sequence stratigraphy of Lake Lisan, the late Pleistocene precursor of the Dead Sea. Quaternary Research 57, 9–21.

Batayneh, A.T., Abueladas, A.A., Moumani, K.A., 2002. Use of ground penetrating radar for assessment of potential sinkhole conditions: an example from Ghor al Haditha area, Jordan. Environmental Geology 41, 977–983.

Beck, B.F., 2003. Sinkholes and the Engineering and Environmental Impacts of Karst, Geotechnical Special Publication 122. American Society of Civil Engineers, RestonVA. 737 pp.

Beck, B.F., Herring, J.G., 2001. Geotechnical and environmental applications of karst geology and hydrology. Proceedings of the 8th Multidisciplinary Conference on Sinkholes and the Engineering and Environmental Impacts of Karst. A.A. Balkema, Rotterdam. 437 pp.

Begin, Z., Nathan, Y., Ehrlich, A., 1980. Stratigraphy and facies distribution in the Lisan Formation new evidence from the area south of the Dead-Sea. Israel Journal of Earth Sciences 29, 182–189.

Ben-Itzhak, L., Gvirtzman, H., 2005. Groundwater flow along and across structural folding: an example from the Judean Desert, Israel. Journal of Hydrology 312, 51–69.

Benson, R.C., Yuhr, L., 1993. Spatial sampling considerations and their applications to characterizing fractured rock and karst system. In: Beck, B.F. (Ed.), Applied Karst Geology. Balkema, Rotterdam, pp. 99–113.

Bernabé, Y., Mok, U., Evans, B., 2003. Permeability–porosity relationship in rocks subjected to various evolution processes. Pure and Applied Geophysics 160, 937–960.

Bodet, L., Galibert, P.Y., Dhemaied, A., Camerlynck, C., Al-Zoubi, A., 2010. Surface-wave profiling for sinkhole hazard assessment along the eastern Dead Sea Shoreline, Ghor Al-Haditha, Jordan. 72nd EAGE Conference & Exibition incorporating EUROPEC 2010, Barcelona M027, p. 4.

Bookman, R., Enzel, Y., Agnon, A., Stein, M., 2004. Late Holocene lake levels of the Dead Sea. Geological Society of America Bulletin 116, 555–571.

Brinkmann, R., Parise, M., Dye, D., 2008. Sinkhole distribution in a rapidly developing urban environment: Hillsborough County, Tampa Bay area, Florida. Engineering Geology 99, 169–184.

Bruner, I., Ezersky, M., Keydar, S., Trachtman, P., 2003. An integrated study of sinkhole development sites using geophysical methods. Geophysical Institute of Israel Report 728/314/03. 36 pp.

Bruthans, J., Filippi, M., Asadi, N., Zare, M., Slechta, S., Churackova, Z., 2009. Surficial deposits on salt diapirs (Zagros Mountains and Persian Gulf Platform, Iran): characterization, evolution, erosion and the influence on landscape morphology. Geomorphology 107, 195–209.

Closson, D., 2005. Structural control of sinkholes and subsidence hazards along the Jordanian Dead Sea coast. Environmental Geology 47, 290–301.

Crawford, N.C., Lewis, M.A., Winter, S.A., Webster, J.A., 1999. Microgravity techniques for subsurface investigations of sinkhole collapses and for detection of groundwater flow paths through karst aquifers. In: Beck, B., Pettit, A., Herring, J.G. (Eds.), Hydrogeology and Engineering Geology of Sinkholes and Karst. Balkema, Rotterdam, pp. 203–218.

De Waele, J., Picotti, V., Zini, L., Cucchi, F., Forti, P., 2009. Karst phenomena in the Cordillera de Sal (Atacama, Chile). In: Rossi, P.L. (Ed.), Geological Constraints on the Onset and Evolution of an Extreme Environment: the Atacama Area: Geoacta Special Publication, 2, pp. 113–127.

Dhemaied, A., 2007. Tomographie seismique d'une zone de subsidence (Sinkhole zone, Ghor Al-Haditha, Jordanie). MSc Report. Paris University, Paris, France.

El-Isa, Z., Rimawi, O., Jarrar, G., Abu-Karaki, N., Taqieddin, S., Atalah, M., Abderahman, N., Al Saed, A., 1995. Assessment of the hazard of subsidence and sinkholes in Ghor Al-Haditha area. Report submitted to Jordan Valley Authority. University of Jordan, Amman. 141 pp.

Eppelbaum, L., Ezersky, M., Al-Zoubi, A., Goldshmidt, V., Legchenko, A., 2008. Study of the factors affecting the karst volume assessment in the Dead Sea sinkhole problem using microgravity field analysis and 3D modeling. Advances in Geosciences 18, 1–19. www.adv-geosci.net/18/1/2008.

Erchul, R.A., 1993. Effective geophysical methods for Virginia karst terrains. In: Beck, B.F. (Ed.), Applied Karst Geology. Balkema, Rotterdam, pp. 131–134.

Ezersky, M., 2003. Study of the shallow subsurface sinkhole hazard areas along Dead Sea shore using geophysical methods. Geophysical Institute of Israel Report 211/247/02. 114 pp.

Ezersky, M., 2006. The geophysical properties of the Dead Sea salt applied to sinkhole problem. Journal of Applied Geophysics 58, 45–58.

Ezersky, M., 2008. Geoelectric structure of the Ein Gedi sinkhole occurrence site at the Dead Sea shore in Israel. Journal of Applied Geophysics 64, 56–69.

Ezersky, M., Legchenko, A., 2008. Sinkhole hazards. Part I. Mapping of the salt in sinkhole hazardous sites along western Dead Sea shore using Seismic Refraction method. NATO Programme Science for Peace, Project SfP 981128. Geophysical Institute of Israel-IRD. Report 232/361/08.

Ezersky, M., Legchenko, A., 2009. TEM resistivity–salinity calibration in the brine saturated sediments along the Dead Sea coast of Israel. 15th EAGE Meeting, Dublin, Ireland, p. 4.

Ezersky, M., Bruner, I., Keydar, S., Trachtman, P., Rybakov, M., 2006. Integrated study of the sinkhole development site using geophysical methods at the Dead Sea western shore. Near Surface Geophysics 4, 335–343.

Ezersky, M., Legchenko, A., Camerlynck, C., Al-Zoubi, A., 2007. The salt formation edge as a major indicator of the sinkhole hazard in the Dead Sea western coast. 13th EAGE Near Surface Meeting & Exhibition, Istanbul, p. 67.

Ezersky, M., Legchenko, A., Kamerlynck, C., Al-Zoubi, A., 2008. Identification of sinkhole development mechanism based on a combined geophysical study in Nahal Hever South area (Dead Sea coast of Israel). Environmental Geology 58, 1123–1141.
Ezersky, M., Legchenko, A., Camerlynck, C., Al-Zoubi, A., Eppelbaum, L., Keidar, S., Baucher, M., Chalikakis, K., 2010. The Dead Sea sinkhole hazard — new findings based on a multidisciplinary geophysical study. Zeitschrift für Geomorphologie N.F. 54, 69–90.
Ford, D.C., Williams, P.W., 2007. Karst Hydrogeology and Geomorphology. Wiley, Chichester. 562 pp.
Frumkin, A., 1994a. Morphology and development of salt caves. National Speleological Society Bulletin 56, 82–95.
Frumkin, A., 1994b. Hydrology and denudation rates of halite karst. Journal of Hydrology 162, 171–189.
Frumkin, A., 1997. The Holocene history of the Dead Sea levels. In: Niemi, T.M., Ben-Avraham, Z., Gat, Y., Niemi, T.M., Ben-Avraham, Z., Gat, Y. (Eds.), The Dead Sea, The Lake and Its Setting. Oxford Univ. Press, Oxford, pp. 237–248.
Frumkin, A., 2001. The cave of the letters sediments — indication of an early phase of the Dead Sea depression? Journal of Geology 109, 79–90.
Frumkin, A., Gvirtzman, H., 2006. Cross-formational rising groundwater at an artesian karstic basin: the Ayalon Saline Anomaly, Israel. Journal of Hydrology 318, 316–333.
Frumkin, A., Raz, E., 2001. Collapse and subsidence associated with salt karstification along the Dead Sea. Carbonates and Evaporites 16, 117–130.
Frumkin, A., Karkanas, P., Bar-Matthews, M., Barkai, R., Gopher, A., Shahack-Gross, R., Vaks, A., 2009a. Gravitational deformations and fillings of aging caves: the example of Qesem karst system, Israel. Geomorphology 106, 154–164.
Frumkin, A., Kofman, L., Ezersky, M., 2009b. Improvement of the reliability of subsurface void detection, including sinkhole development, at the Dead Sea shore area by means of Ground Penetration Radar (GPR). Hebrew University — Technion Research and Development Foundation — Geophysical Institute of Israel, Report MNI-ES-36-2008. . 23 pp.
Galve, J., Gutiérrez, F., Lucha, P., Guerrero, J., Remondo, J., Bonachea, J., Cendrero, A., 2009a. Probabilistic sinkhole modelling for hazard assessment. Earth Surface Processes and Landforms 34, 437–452.
Galve, J.P., Gutiérrez, F., Remondo, J., Bonachea, J., Lucha, P., Cendrero, A., 2009b. Evaluating and comparing methods of sinkhole susceptibility mapping in the Ebro Valley evaporite karst (NE Spain). Geomorphology 111, 160–172.
Garfunkel, Z., Ben-Avraham, Z., 1996. The structure of the Dead Sea Basin. Tectonophysics 266, 155–176.
Goldman, M., Gilad, D., Ronen, A., Melloul, A., 1991. Mapping of sea water intrusion into the coastal aquifer of Israel by the time domain electromagnetic method. Geoexploration 28, 153–174.
Gutiérrez, F., 2009. Hazards associated with karst. In: Alcántara, I., Goudie, A. (Eds.), Geomorphological Hazards and Disaster Prevention. Cambridge University Press, Cambridge, pp. 161–175.
Gutiérrez, F., Galve, J., Guerrero, J., Lucha, P., Cendrero, A., Remondo, J., Bonachea, J., Gutiérrez, M., Sanchez, J.A., 2007. The origin, typology, spatial distribution and detrimental effects of the sinkholes developed in the alluvial evaporite karst of the Ebro River valley downstream of Zaragoza city (NE Spain). Earth Surface Processes and Landforms 32, 912–928.
Gutiérrez, F., Cooper, A., Johnson, K., 2008. Identification, prediction, and mitigation of sinkhole hazards in evaporite karst areas. Environmental Geology 53, 1007–1022.
Kafri, U., Goldman, M., 2005. The use of the time domain electromagnetic method to delineate saline groundwater in granular and carbonate aquifers and evaluate their porosity. Journal of Applied Geophysics 57, 167–178.
Kafri, U., Goldman, M., Lang, B., 1997. Detection of subsurface brines, freshwater bodies and the interface configuration in-between by the time domain electromagnetic method in the Dead Sea Rift, Israel. Environmental Geology 31, 42–49.
Klimchouk, A., 2005. Subsidence hazards in different types of karst: evolutionary and speleogenetic approach. Environmental Geology 48, 287–295.
Klimchouk, A., 2009. Morphogenesis of hypogenic caves. Geomorphology 106, 100–117.
Legchenko, A., Ezersky, M., 2009. Investigation of lateral lithological heterogeneities and groundwater salinity using MRS and TEM methods. 15th EAGE Meeting, Dublin, Ireland, p. A25.
Legchenko, A., Ezersky, M., Camerlynck, C., Al-Zoubi, A., Chalikakis, K., Girard, J.-F., 2008a. Locating water-filled karst caverns and estimating their volume using magnetic resonance soundings. Geophysics 73, 51–61.
Legchenko, A., Ezersky, M., Boucher, M., Camerlynck, C., Al-Zoubi, A., Chalikakis, K., 2008b. Pre-existing caverns in salt formations could be the major cause of sinkhole hazards along the coast of the Dead Sea. Geophysical Research Letters 35, 1–5 L19404.
Legchenko, A., Ezersky, M., Kamerlynck, C., Al-Zoubi, A., Chalikakis, K., 2009. Joint use of TEM and MRS method in complex geological setting. Comptes Rendus Geosciences 341, 908–917.
Lisker, S., Vaks, A., Bar-Matthews, M., Porat, R., Frumkin, A., 2009. Stromatolites in caves of the Dead Sea Fault Escarpment: implications to latest Pleistocene lake levels and tectonic subsidence. Quaternary Science Reviews 28, 80–92.
Loke, M.H., 1999. Electrical imaging surveys for environmental and engineering studies, a practical guide to 2D and 3D surveys. http://www.abem.se. Loke, Penang, 63 pp.
Loke, M.H., Barker, R.D., 1996. Rapid least-squares inversion of apparent resistivity pseudo-sections by a quasi-Newton method. Geophysical Prospecting 44, 131–152.
Lucha, P., Cardona, F., Gutiérrez, F., Guerrero, J., 2008. Natural and human-induced dissolution and subsidence processes in the salt outcrop of the Cardona Diapir (NE Spain). Environmental Geology 53, 1023–1035.
Maimon, O., Lyakhovsky, V., Agnon, A., Abelson, M., 2005. Stability of cavities and formation of sinkholes along the Dead Sea coast. Geological Survey of Israel Report GSI/19/05, Jerusalem. . 65 pp (in Hebrew).
Migowski, C., Stein, M., Prasad, S., Negendank, J., Agnon, A., 2006. Holocene climate variability and cultural evolution in the Near East from the Dead Sea sedimentary record. Quaternary Research 66, 421–431.
Palmer, D., 1986. Refraction Seismic: The Lateral Resolution of Structure and Seismic Velocity. Geophysical Press, London. 269 pp.
Parise, M., De Waele, J., Gutiérrez, F., 2009. Current perspectives on the environmental impacts and hazards in karst. Environmental Geology 58, 235–237.
Reynolds, J.M., 1997. An Introduction to Applied and Environmental Geophysics. Wiley, New York. 796 pp.
Rybakov, M., Goldshmidt, V., Fleischer, L., Rotstein, Y., 2001. Cave detection and 4-D monitoring: a microgravity case history near the Dead Sea. The Leading Edge 20, 896–900.
Shalev, E., Lyakhovsky, V., Yechieli, V., 2006. Salt dissolution and sinkhole formation along the Dead Sea shore. Journal of Geophysical Research 111, B03102.
Shamir, G., 2006. In: Enzel, Y., Agnon, A., Stein, M. (Eds.), The active structures of the DS depression: Geological Society of America Special Paper, 401, pp. 15–32.
Spanbenberg, E., Spanbenberg, U., Heindorf, 1998. An experimental study of transport properties of porous rock salt. Physics and Chemistry of the Earth 23, 367–371.
Stein, M., Torfstein, A., Gavrieli, I., Yechieli, Y., 2010. Abrupt aridities and salt deposition in the post-glacial Dead Sea and their North Atlantic connection. Quaternary Science Reviews 29, 567–575.
Taqieddin, S.A., Abderahman, N.S., Atallah, M., 2000. Sinkhole hazards along the eastern Dead Sea shoreline area, Jordan: a geological and geotechnical consideration. Environmental Geology 39, 1237–1253.
Thomas, B., Roth, M.J.S., 1999. Evaluation of site characterization methods for sinkholes in Pennsylvania and New Jersey. Engineering Geology 52, 147–152.
Yang, M.Z., Drumm, E.C., 2002. Stability evaluation for the sitting of municipal land fills in karst. Engineering Geology 65, 185–195.
Yechieli, Y., 2000. Fresh-saline ground water interface in the western Dead Sea area. Ground Water 38, 615–623.
Yechieli, Y., 2007. Geochemical monitoring of groundwater in boreholes at the Dead Sea coastal area — project of sinkholes. Geological Survey of Israel Report TR-GSI/18/2007.
Yechieli, Y., Wachs, D., Shtivelman, V., Abelson, M., Crouvi, O., Shtivelman, V., Raz, E., Baer, G., 2002. Formation of sinkholes along the shore of the Dead Sea — summary of the first stage of investigation. Geological Survey of Israel Current Research 13, 1–6.
Yechieli, Y., Abelson, M., Bein, A., Crouvi, O., 2006. Sinkhole "swarms" along the Dead Sea coast: reflection of disturbance of lake and adjacent groundwater systems. Geological Society of America Bulletin 118, 1075–1087.
Zhdanov, M.S., Keller, G.V., 1994. The Geoelectrical Methods in Geophysical Exploration. Elsevier, Amsterdam. 873 pp.
Zhou, W., Beck, B.F., Stephenson, J.B., 1999. Application of electrical resistivity tomography and natural-potential technology to deliniate potential sinkhole collapse areas in a covered karst terrane. In: Beck, B.F., Pettit, A.J., Herring, J.G. (Eds.), Hydrogeology and Engineering Geology of Sinkholes and Karst. Balkema, Rotterdam, pp. 187–193.